THEORY INPUT FOR $t\bar{t}j$ EXPERIMENTAL ANALYSES AT THE LHC*

Katharina Voss[a,b], Maria Vittoria Garzelli[a], Sven-Olaf Moch[a]

[a]II. Institut für Theoretische Physik, Universität Hamburg
Luruper Chaussee 149, 22761 Hamburg, Germany
[b]Department für Physik, Universität Siegen, Emmy Noether Campus
Walter Flex Str. 3, 57068 Siegen, Germany

Received 23 December 2021, accepted 27 December 2021, published online 28 February 2022

The precise measurement of the top-quark mass, which is a fundamental SM parameter, constitutes one of the main goals of the LHC top-physics program. One approach to measure this quantity uses the ρ_s distribution, an observable depending on the invariant mass of the $t\bar{t}j$ system. To fully exploit the experimental accuracy achievable in measuring top-quark production cross sections at the LHC, the theory uncertainties associated to these measurements need to be well under control. To this end, we present a study of the effect of varying the theoretical input parameters in the calculation of differential cross sections of the $t\bar{t}j$ process. Thereby, we studied the influence of the jet reconstruction procedure, as well as the effect of various renormalization and factorization scale definitions and different PDF sets. The variation of the R parameter in the jet reconstruction algorithm was found to have negligible influence on the scale variation uncertainty. A strong reduction of scale uncertainties and a better behaviour of the NLO/LO ratios using selected dynamical scales instead of a static one in the high-energy tails of differential distributions was observed. This is particularly interesting in the context of the top-quark mass measurements through the ρ_s distribution, in which the perturbative stability can be improved by applying the proposed dynamical scale definition.

DOI:10.5506/APhysPolBSupp.15.2-A5

1. Introduction

The precise measurement of the properties and interactions of the top-quark, the fundamental particle with the largest mass in the Standard Model (SM), is possible due to the high statistics in top-quark production processes

* Presented at the XLIV International Conference of Theoretical Physics "Matter to the Deepest", 15–17 September, 2021.

available at the Large Hadron Collider (LHC). Besides enabling the investigation of the top-quark Yukawa coupling, the largest Yukawa-coupling in the SM, and testing Beyond the Standard Model theories, measurements of the top-quark SM parameters with unprecedented accuracy can be carried out. In particular, the top-quark mass is linked to fundamental questions in particle physics. For example, the mass of the top-quark m_t, the Higgs-boson m_H and the W-boson m_W are linked through radiative corrections and these mutual dependencies can be exploited to perform a consistency check of the predictions of the SM [1]. Furthermore, the stability or meta-stability of the electroweak vacuum can be inferred from the relations between m_t, m_H, and the strong coupling constant α_s [2–5].

The possibility to extract the top-quark mass through the normalized ρ_s distribution, defined as $\rho_s = 2m_0/\sqrt{m^2_{t\bar{t}j}}$ with $m_0 = 170$ GeV, was first discussed in [6]. This quantity, calculated at NLO in the $t\bar{t}j$ process, was shown to be more sensitive to m_t than the corresponding distribution of $2m_0/\sqrt{m_{t\bar{t}}}$ for the $t\bar{t}$ process. In fact, additional parton radiation in the $t\bar{t}j$ process gives enhanced sensitivity to the mass of the top-quark. As in the extractions of the top-quark mass from cross-section measurements, the mass renormalization scheme can be unambiguously defined when measuring m_t through the ρ_s distribution. Thereby, in [6], it was found that the ρ_s distribution is more sensitive to m_t than the cross-section measurements.

Both ATLAS [7] and CMS [8] performed measurements of the top-quark mass using the ρ_s distribution, where the most recent ATLAS result [7] extracted the pole mass of the top-quark with the value

$$m_t^{\text{pole}} = 171.1 \pm 0.4\,(\text{stat.}) \pm 0.9\,(\text{syst.})^{+0.7}_{-0.3}\,(\text{theo.})\ \text{GeV}\,. \tag{1}$$

The theoretical uncertainty in the extraction is sizeable, which is dominated by the scale variation uncertainty $(+0.6, -0.2)$ GeV, while the parton distribution function (PDF) and α_s uncertainty leads only to an uncertainty of ± 0.2 GeV in the m_t^{pole} determination. Therefore, we carried out an investigation of the theoretical uncertainties in the $t\bar{t}j$ process and the possibility to improve the perturbative stability through informed choices of the theoretical input in the calculation and in the analysis procedure.

A study of the $t\bar{t}j$ production process is furthermore interesting, since a substantial fraction of $t\bar{t}$ events at the LHC is accompanied by an additional jet (40% of $t\bar{t}$ events, if $p_T^j > 40$ GeV at $\sqrt{s} = 13$ TeV [9]), and this process constitutes the dominant background to Higgs production in vector boson fusion (VBF), see *e.g.* [10].

The first NLO calculation of $t\bar{t}j$ production at a hadron collider was presented in [11], where stable top-quarks were considered. In [12], the LO top-quark decay was included and later, in [13], the NLO QCD off-shell

effects in the fully leptonic decay of the top-quark were considered. The combination of the NLO $t\bar{t}j$ calculation and a parton shower (PS) was first presented in [14] using hard scattering amplitudes from HELAC-NLO [15] and the PS matching method implemented in the POWHEG-BOX [16]. A second implementation, using the virtual corrections from [11] and Born and real squared amplitudes from Madgraph [17], in the POWHEG-BOX, called in the following ttbarj V1 [18] was published shortly afterwards. In the study presented here, the ttbarj V2 version was used, where in contrast to ttbarj V1, all amplitudes are calculated with OpenLoops2 [19], and the calculation can be parallelized, leading to strongly reduced computation time.

2. Input parameters of the calculation

The presented predictions are obtained with na NLO calculation of the $t\bar{t}j$ process at a center-of-mass energy of $\sqrt{s} = 13$ TeV. The pole mass of the top-quark is set to $m_t^{\text{pole}} = 172$ GeV and stable top-quarks are considered. As a PDF set and for the evolution of the strong coupling constant α_s, the CT18NLO PDF set [20] was used as default. To estimate the scale variation uncertainty, the seven-point scale variation method was used, varying the renormalization $\mu_R = K_R \mu_0$ and factorization scale $\mu_F = K_F \mu_0$ in the range of

$$(K_R, K_F) \in \{(0.5, 0.5), (0.5, 1), (1, 0.5), (1, 1), (1, 2), (2, 1), (2, 2)\}\,. \qquad (2)$$

In the analysis, at least one jet with a transverse momentum $p_T^j > 30$ GeV and a pseudorapidity $|\eta_j| < 2.4$ was required, where the jets are reconstructed with the anti-k_T jet clustering algorithm from FastJet [21] using the E-recombination scheme and the $R = 0.4$ value.

In the calculation, we used different definitions of the central scale, as it was found in [13] that dynamical scales were able to better describe the high-energy tails of various NLO differential distributions for $pp \to t\bar{t}j$ in fully leptonic decay compared to the static scale $\mu_0 = m_t^{\text{pole}}$. In contrast to [13], our study was carried out with more inclusive analysis cuts and stable top-quarks. This is owed to the refined techniques of the experimental collaborations to unfold to parton level. We considered four scale definitions, a static scale $\mu_0 = m_t^{\text{pole}}$ and three dynamical scales $\mu_0 = m_{t\bar{t}j}^{\text{B}}/2$, $H_T^{\text{B}}/2$ and $H_T^{\text{B}}/4$, where

$$\begin{aligned} m_{t\bar{t}j} &= \sqrt{\left(p_t^{\text{B}} + p_{\bar{t}}^{\text{B}} + p_j^{\text{B}}\right)^2}\,, \\ H_T^{\text{B}} &= \sqrt{{p_{T,t}^{\text{B}}}^2 + {m_t^{\text{pole}}}^2} + \sqrt{{p_{T,\bar{t}}^{\text{B}}}^2 + {m_t^{\text{pole}}}^2} + p_{T,j}^{\text{B}}\,. \end{aligned} \qquad (3)$$

The superscript "B" implies that the kinematic variables are reconstructed at the underlying Born level in the POWHEG-BOX.

3. Evaluation of the scale variation uncertainty

3.1. Scale variation uncertainty in the ρ_s distribution

As the ρ_s distribution provides a possibility to measure the top-quark mass and the theoretical uncertainty in this extraction is sizeable, as anticipated in Section 1, this distribution is discussed in detail in the following.

In Fig. 1, the NLO ρ_s distribution is shown for the static scale $\mu_0 = m_t^{\rm pole}$ and the dynamical scales $\mu_0 = m^{\rm B}_{t\bar{t}j}/2, H^{\rm B}_{\rm T}/2$ and $H^{\rm B}_{\rm T}/4$. Besides the prediction obtained with $\mu_{\rm R} = \mu_{\rm F} = \mu_0$ also the six scale variation graphs, generated by varying $K_{\rm R}$ and $K_{\rm F}$ appearing in $(\mu_{\rm R}, \mu_{\rm F}) = (K_{\rm R}, K_{\rm F})\mu_0$ with values $K_{\rm R}, K_{\rm F} \in \{0.5, 1, 2\}$, leaving out the extreme combinations (0.5,2) and (2,0.5), are shown explicitly. In the case of the static scale $\mu_0 = m_t^{\rm pole}$ (left panel), a large spread in the graphs, from which the scale variation

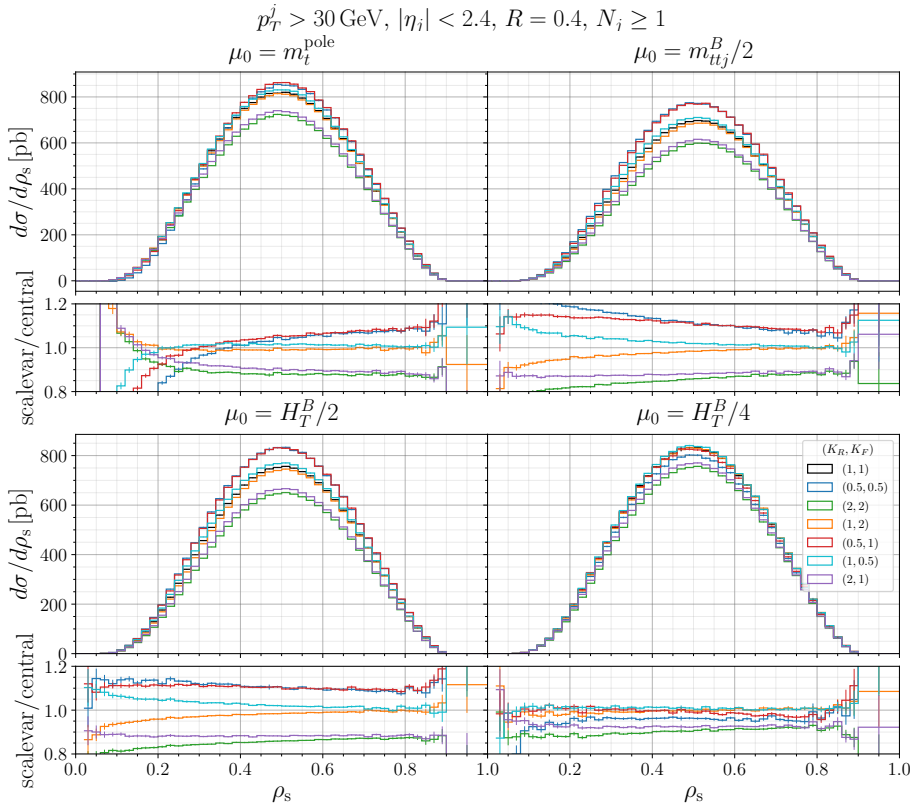


Fig. 1. NLO differential cross section of the process $pp \to t\bar{t}j + X$ at $\sqrt{s} = 13$ TeV as a function of ρ_s obtained with the scales $\mu_0 = m_t^{\rm pole}$, $m^{\rm B}_{t\bar{t}j}/2$ (top, from left to right), $H^{\rm B}_{\rm T}/2$ and $H^{\rm B}_{\rm T}/4$ (bottom, from left to right). The seven scale variation graphs are drawn explicitly, while in each of the lower insets the ratios of these with the prediction obtained with $K_{\rm R} = K_{\rm F} = 1$ (black) are shown.

uncertainty band is built, is observed at low ρ_{s}, which corresponds to large values of $m_{t\bar{t}j}$ and as such to the high-energy region. Furthermore, a crossing of the scale variation bands occurs using the static scale for $0.1 \lesssim \rho_{\mathrm{s}} \lesssim 0.3$. Such a pronounced behaviour is not seen using the dynamical scales and the scale variation induces a smaller shape variation of the ρ_{s} distribution in these cases. This leads to a strongly reduced scale variation uncertainty, when comparing the normalized ρ_{s} distributions. In this case, each distribution obtained with different μ_{R}, μ_{F} values is normalized by the total cross section calculated with these input values. As an example, the normalized ρ_{s} distribution including the seven-point scale variation uncertainty band is shown in Fig. 2 for the static scale $\mu_0 = m_t^{\mathrm{pole}}$ (black) and the dynamical scale $\mu_0 = H_{\mathrm{T}}^{\mathrm{B}}/4$ (blue), which was found to be the dynamical scale leading to the smallest scale variation uncertainty. The strong reduction of the scale variation uncertainty bands is especially visible in the lower two ratio plots, in which the scale variation bands are rescaled by the corresponding nominal distribution. Besides showing a smaller scale uncertainty in the region of low ρ_{s} values, in which the description with the static scale is problematic, a smaller uncertainty band is obtained also in the bulk of the distribution.

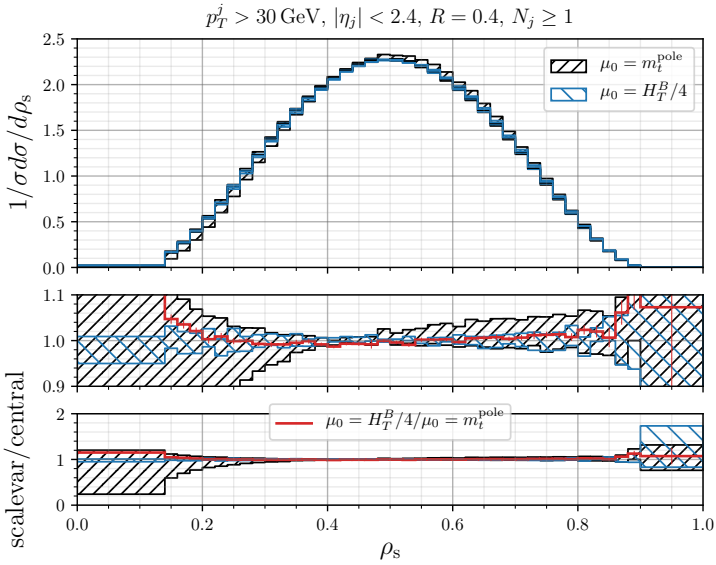


Fig. 2. NLO differential cross section of the process $pp \to t\bar{t}j + X$ at $\sqrt{s} = 13$ TeV and the seven-point scale uncertainty band as a function of ρ_{s} obtained with the static scale $\mu_0 = m_t^{\mathrm{pole}}$ (black) and the dynamical scale $\mu_0 = H_{\mathrm{T}}^{\mathrm{B}}/4$ (blue). The ratio plots in the lower two panels show the scale variation uncertainty bands normalized to the distribution obtained with $K_{\mathrm{R}} = K_{\mathrm{F}} = 1$, while using the corresponding scale definition. Thereby, the two ratio plots differ only in the displayed y-axis range. The ratio of the two nominal predictions is shown by the red graph.

A further possibility to evaluate the most preferable choice of the scale is to compare the calculation of the ρ_s distribution at different perturbative orders, explicitly in this case the ρ_s distribution calculated at LO and NLO. A central scale choice, which leads to small high-order corrections is desirable, as it can indicate that the calculation will not deviate from the current NLO result in higher, yet uncalculated orders. This comparison, including also the seven-point scale variation uncertainty bands at either LO (black) or NLO (blue), is shown in Fig. 3. Especially, comparing the lower ratio plots, in which both seven-point scale variation bands are rescaled by the LO central scale prediction, the two scales $\mu_0 = m_t^{\text{pole}}$ and $\mu_0 = m_{t\bar{t}j}^{\text{B}}/2$ seem problematic, since the NLO and LO scale variation bands only slightly

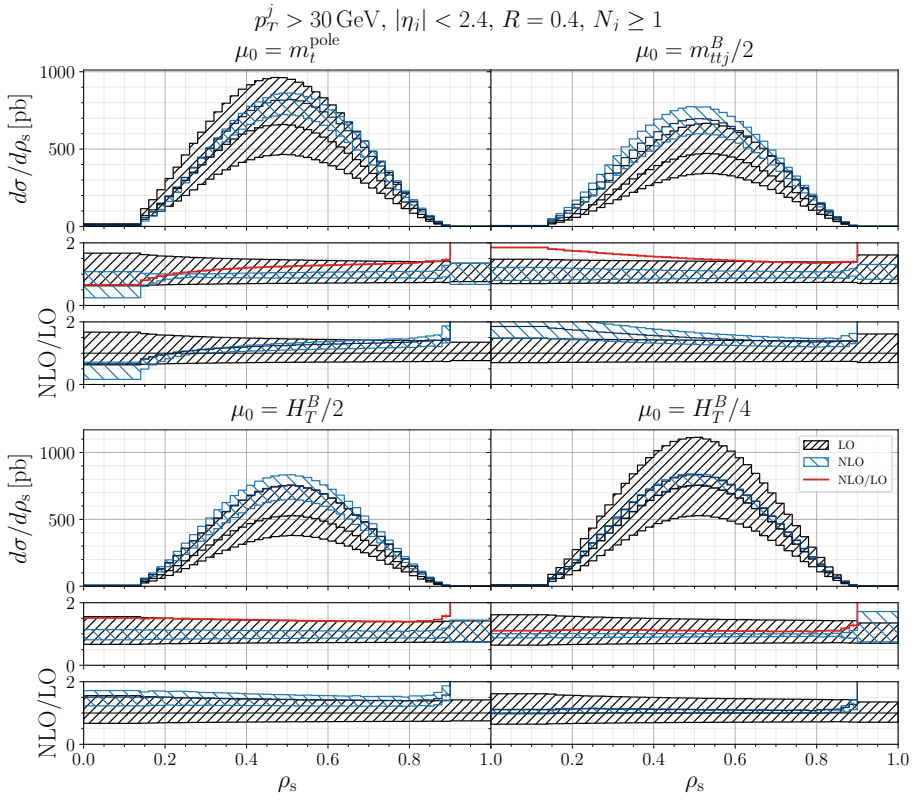


Fig. 3. NLO (blue) and LO (black) differential cross section of the process $pp \to t\bar{t}j + X$ at $\sqrt{s} = 13$ TeV as a function of ρ_s obtained with the scales $\mu_0 = m_t^{\text{pole}}$, $m_{t\bar{t}j}^{\text{B}}/2$ (top, from left to right), $H_{\text{T}}^{\text{B}}/2$ and $H_{\text{T}}^{\text{B}}/4$ (bottom, from left to right). The seven-point scale variation uncertainty bands are drawn, which are rescaled in the middle ratio plot to either the LO or NLO central scale prediction, while in the lower ratio plot, both NLO and LO scale variation bands are rescaled by the LO central scale prediction.

overlap in the high-energy region. On the other hand, the description using $\mu_0 = H_{\mathrm{T}}^{\mathrm{B}}/2$ and $\mu_0 = H_{\mathrm{T}}^{\mathrm{B}}/4$ shows a more uniform differential $\mathcal{K}$ factor, depicted with the red line in the middle plot of Fig. 3. The differential $\mathcal{K}$ factor using $\mu_0 = H_{\mathrm{T}}^{\mathrm{B}}/4$ is close to one, which was the original motivation to investigate this dynamical scale, since the ratio of the integrated cross section calculated at NLO and LO was also found to be near one. A similar behaviour in the high-energy tails of differential distributions was also found for other observables and agrees with the findings in [13].

3.2. Influence of the R parameter on the scale variation uncertainty

Investigating further the static scale $\mu_0 = m_t^{\mathrm{pole}}$ and the two dynamical scales, which seem to be preferable considering the results of Section 3.1, namely $\mu_0 = H_{\mathrm{T}}^{\mathrm{B}}/2$ and $\mu_0 = H_{\mathrm{T}}^{\mathrm{B}}/4$, the influence of the choice of the R parameter in the anti-k_{T} jet clustering algorithm is studied. Two values of this parameter are considered, the default value of $R = 0.4$ and an additional value of $R = 0.8$, for which the experimental analyses have also investigated reconstruction efficiencies and Monte Carlo to data comparison in order to determine the systematic uncertainties.

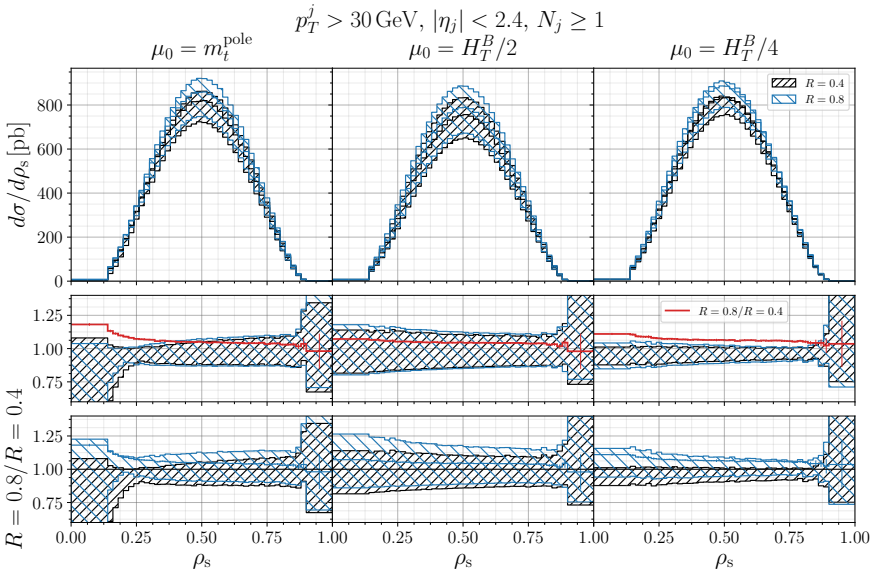


Fig. 4. NLO differential cross section of the process $pp \to t\bar{t}j + X$ at $\sqrt{s} = 13$ TeV as a function of ρ_{s} obtained with the scales $\mu_0 = m_t^{\mathrm{pole}}$, $H_{\mathrm{T}}^{\mathrm{B}}/2$ and $H_{\mathrm{T}}^{\mathrm{B}}/4$ (from left to right) using the anti-k_{T} jet clustering algorithm with either $R = 0.4$ (black) or $R = 0.8$ (blue). The seven-point scale variation uncertainty band is drawn, which is rescaled in the middle ratio plot to either central scale prediction (using either R value), while in the lower ratio plot, both scale variation bands are rescaled by the central scale prediction obtained by setting R to the default value of $R = 0.4$.

As shown in Fig. 4, using the dynamical scales, the choice of the R parameter has only a minor influence on the size of the scale variation uncertainty, while the predictions obtained with the static scale show a slightly reduced scale uncertainty in the high-energy tails with the larger $R = 0.8$ value. However, as elaborated in the previous section, this phase-space region seems not to be well described using the static scale. Using either scale definition, the differential cross sections show larger values using the larger R parameter, which can be advantageous in statistically limited analyses. The same features, described here for the ρ_{s} distribution, were also found for several other differential cross sections.

4. Evaluation of the PDF uncertainty

As the predictions obtained with the scale choice $\mu_0 = H_{\mathrm{T}}^{\mathrm{B}}/4$ were found to have desirable features in Section 3, leading to a small scale variation uncertainty, overlapping NLO and LO scale variation bands and a stable description of the high-energy region, the PDF uncertainties using this same scale, are investigated in the following. Thereby, four modern PDF sets are compared, *i.e.* the default PDF set used in this study CT18NLO and the ABMP16 [22], MSHT20 [23], and NNPDF3.1 [24] NLO sets. The PDF uncertainties were calculated according to the recommendations given by the authors of each PDF fit. Due to the large computational effort needed to calculate the corresponding distributions for each eigenvector set of the different PDF fits, the approximation of using LO partonic cross sections in combination with NLO PDF sets instead of NLO partonic cross sections to estimate the NLO PDF uncertainty, is used in the presented predictions. The validity of this approximation was tested by comparing the percentage size of the PDF uncertainty bands in several differential distributions using the NLO and LO partonic cross section and finding very good agreement. This study was performed using as a central scale $\mu_0 = H_{\mathrm{T}}^{\mathrm{B}}/2$ and a further comparison of the percentage size of the PDF uncertainty bands obtained with $\mu_0 = H_{\mathrm{T}}^{\mathrm{B}}/4$ and $\mu_0 = H_{\mathrm{T}}^{\mathrm{B}}/2$ also showed very similar results.

In Fig. 5, we present the ρ_{s} distribution calculated with the LO partonic matrix elements using $\mu_0 = H_{\mathrm{T}}^{\mathrm{B}}/4$ and the four different NLO PDF sets described above to approximate the NLO PDF uncertainties. In the bulk of the ρ_{s} distribution, good agreement between the predictions from the different PDF sets is observed, while in the region of low ρ_{s} differences are seen, which are not covered by the PDF uncertainty bands. This was found to be caused by the differences between the predicted gluon PDFs at large momentum fractions x, which are shown in Fig. 6 for $Q^2 = m_t^{\mathrm{pole}\,2} = (172\ \mathrm{GeV})^2$. The minimal $x_{\mathrm{min}} = \min(x_1, x_2)$ and the maximal momentum fraction $x_{\mathrm{max}} = \max(x_1, x_2)$ carried by the incoming partons have a peak

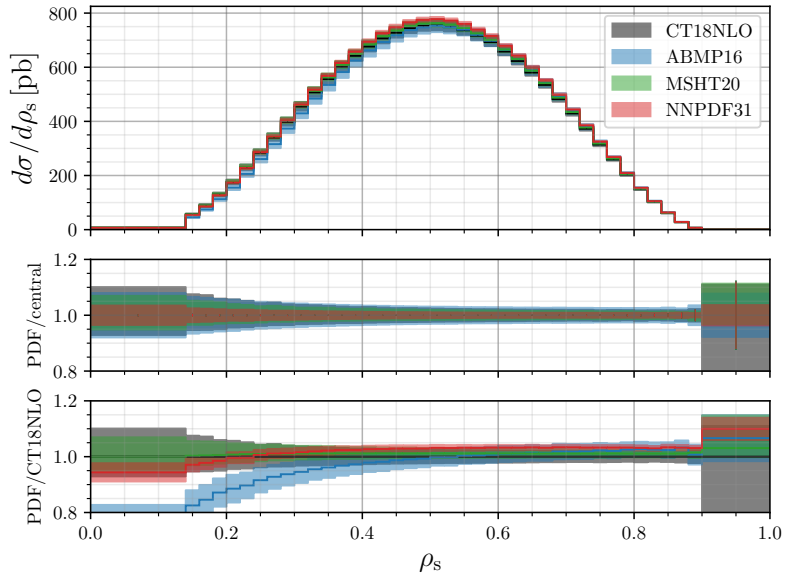


Fig. 5. Approximation of the NLO PDF uncertainties, as described in Section 4, for the ρ_s distribution of the process $pp \to t\bar{t}j + X$ at $\sqrt{s} = 13$ TeV obtained with the dynamical scale $\mu_0 = H_T^B/4$. Four NLO PDF sets were studied, CT18NLO (black), ABMP16 (blue), MSHT20 (green), and NNPDF3.1 (red), and the PDF uncertainties calculated as recommended by the authors of the corresponding PDF fits.

at $x_{\min} = 0.02$ and $x_{\max} = 0.07$, when requiring that the event leads to a ρ_s value in the bulk of the distribution, explicitly in the interval of $\rho_s \in [0.14, 0.65]$. For these values, the gluon PDFs in Fig. 6 show good agreement among each other. On the other hand, in the region of low ρ_s, $\rho_s \in [0, 0.14]$, peaks are observed for $x_{\min} = 0.15$ and $x_{\max} = 0.25$. In fact, for this range of x-values, a clear deviation of the predictions from different PDF sets is found, which is greater than the corresponding PDF uncertainties associated with each PDF fit.

Finally, in Fig. 7, the normalized ρ_s distribution is shown, which was obtained with the scale $\mu_0 = H_T^B/4$. Both the approximate NLO PDF uncertainty (black), calculated as described above with the LO partonic cross sections and the NLO PDF set, and the NLO scale variation uncertainty bands (blue), are depicted. The PDF uncertainty in the bulk of the normalized ρ_s distribution is of similar size as the scale variation uncertainty for the choice of the dynamical scale $\mu_0 = H_T^B/4$.

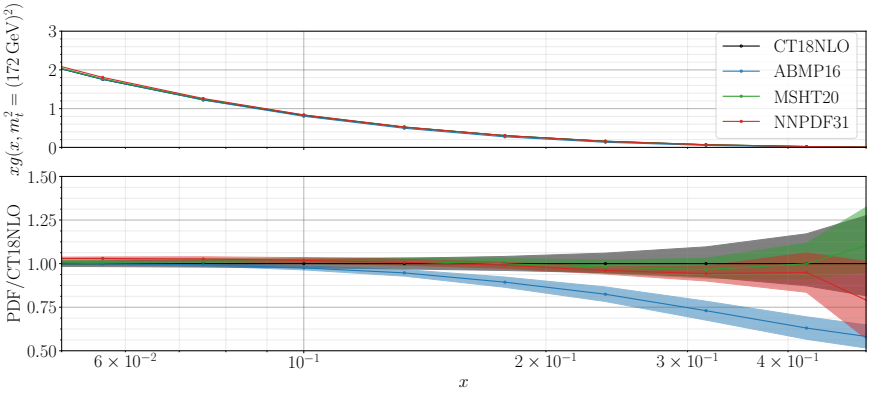


Fig. 6. Gluon PDFs as a function of the momentum fraction x, while setting $Q^2 = (m_t^{\mathrm{pole}})^2 = (172\ \mathrm{GeV})^2$. Four NLO PDF sets were considered, CT18NLO (black), ABMP16 (blue), MSHT20 (green), and NNPDF3.1 (red), and the PDF uncertainties calculated as recommended by the authors of the corresponding PDF fits.

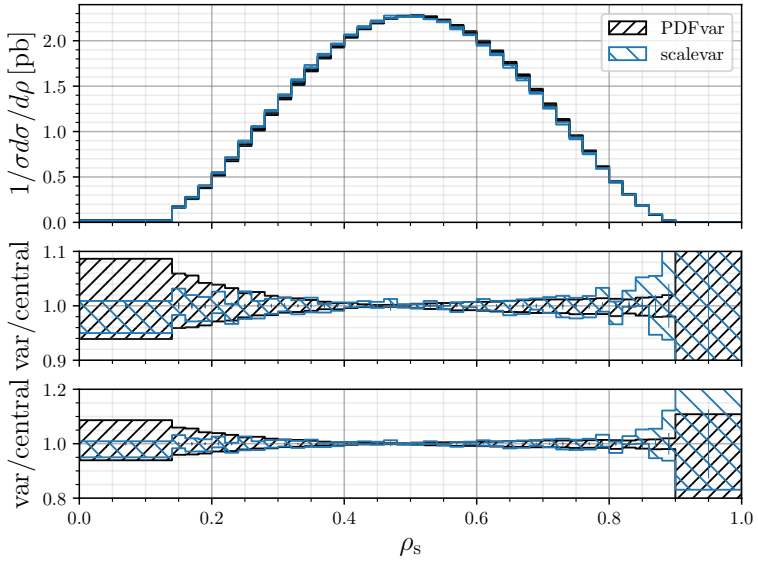


Fig. 7. Normalized NLO differential cross section of the process $pp \to t\bar{t}j + X$ at $\sqrt{s} = 13$ TeV as a function of ρ_{s} obtained with the dynamical scale $\mu_0 = H_{\mathrm{T}}^{\mathrm{B}}/4$. The NLO seven-point scale variation uncertainty band (blue) and the approximate NLO PDF uncertainty band (black) are shown, which are rescaled in the lower panel to the nominal distributions (corresponding to LO for approximate NLO PDF uncertainty and NLO for scale variation uncertainty).

5. Conclusions

We investigated the theoretical uncertainties in the $t\bar{t}j$ process especially focusing on the ρ_{s} distribution, which can be used to extract the top-quark mass from experimental measurements. Thereby, we studied different scale definitions and found, in agreement with [13], that a dynamical scale is better suited to describe this process in the high-energy tails, compared to the static scale $\mu_0 = m_t^{\mathrm{pole}}$. This is seen by the reduced width of the scale variation uncertainty bands in this kinematic region. Furthermore, a strong reduction of scale uncertainty in the normalized ρ_{s} distribution was observed using the dynamical instead of the static scale definition, due to the smaller shape variation induced by the scale variation. When comparing the dynamical scales, by considering the NLO and LO scale variation uncertainty bands, the $\mu_0 = H_{\mathrm{T}}^{\mathrm{B}}/2$ and $\mu_0 = H_{\mathrm{T}}^{\mathrm{B}}/4$ scales are found to be preferable over $\mu_0 = m_{t\bar{t}j}^{\mathrm{B}}/2$, as overlapping bands are found over the whole ρ_{s} range in the case of the former two. Owing to the strongly reduced scale variation uncertainty in the normalized ρ_{s} distribution using $\mu_0 = H_{\mathrm{T}}^{\mathrm{B}}/4$, this theoretical uncertainty is similar in size to the PDF variation uncertainty in the kinematical region of interest for the experimental extraction of m_t^{pole}. Also, the influence of the R-parameter in the anti-k_{T} jet clustering algorithm was investigated and was found to be negligible on the scale variation uncertainty when using the preferred dynamical scales $\mu_0 = H_{\mathrm{T}}^{\mathrm{B}}/2$ and $\mu_0 = H_{\mathrm{T}}^{\mathrm{B}}/4$.

We are grateful to Simone Alioli and Alessandro Gavardi for sharing with us their latest POWHEG-BOX implementation of the $t\bar{t}j$ hadroproduction process and for useful discussions, and to Adrian Irles and Peter Uwer for further discussions, suggestions, and cross-checks. The work of M.V.G. and S.-O.M. was partially supported by the Bundesministerium für Bildung and Forschung (contract 05H21GUCCA). The work of K.V. was partially funded by the House of Young Talents Siegen.

REFERENCES

[1] M. Awramik, M. Czakon, A. Freitas, G. Weiglein, «Precise prediction for the W-boson mass in the standard model», *Phys. Rev. D* **69**, 053006 (2004), arXiv:hep-ph/0311148.

[2] F. Bezrukov, M.Yu. Kalmykov, B.A. Kniehl, M. Shaposhnikov, «Higgs boson mass and new physics», *J. High Energy Phys.* **2012**, 140 (2012), arXiv:1205.2893 [hep-ph].

[3] G. Degrassi *et al.*, «Higgs mass and vacuum stability in the Standard Model at NNLO», *J. High Energy Phys.* **2012**, 98 (2012), arXiv:1205.6497 [hep-ph].

[4] S. Alekhin, A. Djouadi, S. Moch, «The top quark and Higgs boson masses and the stability of the electroweak vacuum», *Phys. Lett. B* **716**, 214 (2012), arXiv:1207.0980 [hep-ph].

[5] A.V. Bednyakov, B.A. Kniehl, A.F. Pikelner, O.L. Veretin, «Stability of the Electroweak Vacuum: Gauge Independence and Advanced Precision», *Phys. Rev. Lett.* **115**, 201802 (2015), arXiv:1507.08833 [hep-ph].

[6] S. Alioli *et al.*, «A new observable to measure the top-quark mass at hadron colliders», *Eur. Phys. J. C* **73**, 2438 (2013), arXiv:1303.6415 [hep-ph].

[7] ATLAS Collaboration, «Measurement of the top-quark mass in $t\bar{t}+1$-jet events collected with the ATLAS detector in pp collisions at $\sqrt{s}=8$ TeV», *J. High Energy Phys.* **2019**, 150 (2019), arXiv:1905.02302 [hep-ex].

[8] CMS Collaboration, «Determination of the normalised invariant mass distribution of $t\bar{t}$+jet and extraction of the top quark mass», Tech. Rep. CMS-PAS-TOP-13-006, CERN, Geneva, 2016.

[9] M. Kraus, «NLO QCD off-shell effects for top pair production with a jet in the dilepton channel», arXiv:1608.05296 [hep-ph].

[10] D.L. Rainwater, D. Zeppenfeld, «Observing $H\to W^*W^*\to e^\pm\mu^\mp p_{\rm T}$ in weak boson fusion with dual forward jet tagging at the CERN LHC», *Phys. Rev. D* **60**, 113004 (1999), arXiv:hep-ph/9906218; *Erratum ibid.* **61**, 099901 (2000).

[11] S. Dittmaier, P. Uwer, S. Weinzierl, «Hadronic top-quark pair production in association with a hard jet at next-to-leading order QCD: phenomenological studies for the Tevatron and the LHC», *Eur. Phys. J. C* **59**, 625 (2009), arXiv:0810.0452 [hep-ph].

[12] K. Melnikov, M. Schulze, «NLO QCD corrections to top quark pair production in association with one hard jet at hadron colliders», *Nucl. Phys. B* **840**, 129 (2010), arXiv:1004.3284 [hep-ph].

[13] G. Bevilacqua, H.B. Hartanto, M. Kraus, M. Worek, «Top Quark Pair Production in Association with a Jet with Next-to-Leading-Order QCD Off-Shell Effects at the Large Hadron Collider», *Phys. Rev. Lett.* **116**, 052003 (2016), arXiv:1509.09242 [hep-ph].

[14] A. Kardos, C.G. Papadopoulos, Z. Trócsányi, «Top quark pair production in association with a jet at NLO accuracy with parton showering», *Phys. Lett. B* **705**, 76 (2011), arXiv:1101.2672 [hep-ph].

[15] A. van Hameren, C.G. Papadopoulos, R. Pittau, «Automated one-loop calculations: a proof of concept», *J. High Energy Phys.* **2009**, 106 (2009), arXiv:0903.4665 [hep-ph].

[16] S. Alioli, P. Nason, C. Oleari, E. Re, «A general framework for implementing NLO calculations in shower Monte Carlo programs: the POWHEG BOX», *J. High Energy Phys.* **2010**, 43 (2010), arXiv:1002.2581 [hep-ph].

[17] J. Alwall *et al.*, «MadGraph/MadEvent v4: the new web generation», *J. High Energy Phys.* **2007**, 028 (2007), arXiv:0706.2334 [hep-ph].

[18] S. Alioli, S.-O. Moch, P. Uwer, «Hadronic top-quark pair-production with one jet and parton showering», *J. High Energy Phys.* **2012**, 137 (2012), arXiv:1110.5251 [hep-ph].

[19] F. Buccioni *et al.*, «OpenLoops 2», *Eur. Phys. J. C* **79**, 866 (2019), arXiv:1907.13071 [hep-ph].

[20] T.-J. Hou *et al.*, «New CTEQ global analysis of quantum chromodynamics with high-precision data from the LHC», *Phys. Rev. D* **103**, 014013 (2021), arXiv:1912.10053 [hep-ph].

[21] M. Cacciari, G.P. Salam, G. Soyez, «FastJet user manual (for version 3.0.2)», *Eur. Phys. J. C* **72**, 1896 (2012), arXiv:1111.6097 [hep-ph].

[22] S. Alekhin, J. Blümlein, S. Moch, «NLO PDFs from the ABMP16 fit», *Eur. Phys. J. C* **78**, 477 (2018), arXiv:1803.07537 [hep-ph].

[23] S. Bailey *et al.*, «Parton distributions from LHC, HERA, Tevatron and fixed target data: MSHT20 PDFs», *Eur. Phys. J. C* **81**, 341 (2021), arXiv:2012.04684 [hep-ph].

[24] R.D. Ball *et al.*, «Parton distributions from high-precision collider data», *Eur. Phys. J. C* **77**, 663 (2017), arXiv:1706.00428 [hep-ph].